Broadband low-dispersion diffraction of femtosecond pulses from photorefractive quantum wells

M. Dinu

Department of Physics, Purdue University, West Lafayette, Indiana 47907-1396

K. Nakagawa

Department of Computer and Systems Engineering, Faculty of Engineering, Kobe University, Kobe, Japan

M. R. Melloch and A. M. Weiner

School of Electrical and Computer Engineering, Purdue University, West Lafayette, Indiana 47907-1285

D. D. Nolte

Department of Physics, Purdue University, West Lafayette, Indiana 47907-1396

Received September 7, 1999; revised manuscript received January 24, 2000

Photorefractive quantum wells operating by means of the Franz–Keldysh effect were designed to diffract a bandwidth of approximately 8 nm, nearly matching that of 100-fs pulses, with little dispersion in the diffracted pulses. Large diffraction bandwidths are engineered by adjustment of the well width of the quantum wells in a specific nonuniform distribution across the thickness of the device. The causal relationship between the real and the imaginary parts of the refractive index leads to an excitonic spectral phase with linear dependence on wavelength, resulting in almost distortion-free diffraction. These features render photorefractive quantum-well devices suitable candidates for femtosecond pulse-shaping and spectral holography applications, without the previous bandwidth limitations. © 2000 Optical Society of America
[S0740-3224(00)00806-7]

OCIS codes: 190.5330, 190.5970, 260.2030, 190.7110, 230.0250.

1. INTRODUCTION

Photorefractive quantum wells (PRQW's) have high sensitivities, small saturation intensities, and short response times compared with those of bulk photorefractives.[1] These properties are desirable in applications such as dynamic femtosecond pulse shaping and femtosecond spectral holography.[2,3] PRQW's have been used to study femtosecond diffraction from quasi-static excitonic gratings,[4] pulse shaping[5] and femtosecond processing.[6] Adaptive applications include all-order dispersion compensation.[7] PRQW's functioning at the resonant exciton wavelength have been shown to be useful for a wide variety of narrow-band applications, such as optical coherence tomography,[8,9] optical image processing,[10] and ultrasound detection.[11] However, these devices previously suffered from a limited diffraction bandwidth that resulted from the narrow linewidth of the resonant electro-optic response of quantum-confined excitons in quantum wells. The narrow bandwidth can limit the usefulness of the devices for femtosecond applications. The operating bandwidth of a typical GaAs/AlGaAs photorefractive multiple-quantum-well (MQW) device at room temperature, because of phonon broadening of the excitonic transition and inhomogeneous broadening that results from well thickness and well–barrier interface disordering, is typically of the order of 4 nm. The size of this bandwidth must be compared with that of a 100-fs pulse, which is approximately 10 nm (or ≈5 THz) at 800 nm.

The large bandwidths of ultrafast pulses could conceivably be of use in fiber-optic communications, and there is ongoing research for the development of simple and robust pulse-shaping techniques and appropriate materials for use in high-bit-rate communications.[12] Pulse shaping and control of ultrafast pulses are of interest not only from the practical point of view of implementing high-bit-rate communications by use of ultrafast laser sources[13] but also more fundamentally for realizing processes such as coherent control of quantum dynamics and chemical reaction pathways.[14] A variety of optical materials, including pixelated liquid-crystal arrays,[2] rf-driven acousto-optical modulators,[15] charge-transfer polymers,[16] and semiconductor waveguide modulators,[17] have been used for femtosecond pulse shaping and ultrafast pulse switching. Bandgap engineered broadband semiconductor MQW devices have been used as fast saturable absorbers for the Kerr-lens mode locking of solid-state lasers.[18,19] PRQW's operate in a different regime from fast saturable absorber MQW's, in which the nonlinearity is due to band filling. The operation of photorefractive MQW's relies on the resonant electro-optic response at the exciton transi-

tion, and the diffractive response of these devices is intrinsically of limited bandwidth. Therefore the diffractive bandwidth of a PRQW has to be specifically engineered for femtosecond applications.

We demonstrate the feasibility of achieving large diffraction bandwidths in photorefractive four-wave mixing by use of photorefractive MQW devices. The Kramers–Kronig relationship between the change in absorption and index that is due to applied electric fields ensures a nearly linear dependence on frequency of the spectral phase of the diffracted pulses. Therefore the large changes in the spectral phase in the vicinity of the excitonic resonance do not preclude transform-limited diffraction. In Section 2 of this paper we describe the optical properties and electro-optic response of PRQW devices and the principles of broadband device design. In Section 3 we present the results of femtosecond diffraction experiments, and in Section 4 we discuss the linearity of the excitonic spectral phase in PRQW's, which is of paramount importance for achieving broadband dispersionless diffraction.

2. BROAD-BANDWIDTH QUANTUM-WELL DESIGN AND ELECTRO-OPTIC CHARACTERIZATION

The photorefractive effect[1] is a low-intensity nonlocal optical nonlinearity that is sensitive to spatial variations in optical illumination: A spatially variable pattern of photogenerated charge leads, by means of charge transport and subsequent charge trapping at deep level defects, to a space-charge field. In PRQW's a resonant electro-optic effect converts the space-charge field grating into a spatially varying pattern of the complex refractive index. If the spatial variation is one dimensional, the complex index grating is

$$\tilde{n}(x, \omega) = \tilde{n}(\omega) + \Delta\tilde{n}(\omega) f(Kx + \phi), \tag{1}$$

where $\tilde{n}(\omega) = n(\omega) + i\alpha(\omega)/2k$ is the complex refractive index, α is the absorption coefficient, n is the refractive index, and k is the light-wave vector in vacuum; f represents the spatial variation of the interference grating. The grating vector is K, and ϕ is the phase shift, which is generally nonzero, between the intensity and index gratings. The electro-optic effect that is responsible for the induced grating in quantum wells can be either the Franz–Keldysh effect or the Stark effect, depending on the orientation of the applied electric field relative to the quantum-well plane. In what follows, we focus on the Franz–Keldysh effect, in which the electric field is applied parallel to the plane of the quantum wells. Electroabsorption $\Delta\alpha$ and electrorefraction Δn vary quadratically with the applied electric field for small applied fields.

The electric field of a short pulse has the form $E(t) = e(t)\exp(-i\omega_c t)$, where $e(t)$ is the pulse's temporal envelope and ω_c is the pulse's central frequency. In the spectral domain the electric field $E(\omega)$ is the Fourier transform of $E(t)$. Let a pulse $E_{\text{in}}(\omega)$ be incident upon the thin-film quantum well and assume that the grating function $f(Kx + \phi)$ is a harmonic function (this is a good approximation, because the strongest diffraction occurs from the fundamental harmonic of a periodic grating). At the exit plane the electric field of the transmitted pulse (in all orders) is

$$E_{\text{out}}(\omega) = E_{\text{in}}(\omega)\exp(i\tilde{n}kL)\exp(i\Delta\tilde{n}kL)\cos(Kx + \phi), \tag{2}$$

where L is the thickness of the device. The output electric field is expanded as[20]

$$E_{\text{out}}(\omega) = E_{\text{in}}(\omega)\exp(i\tilde{n}kL)\sum_{m=-\infty}^{+\infty} i^m J_m[\Delta\tilde{n}(\omega)kL]. \tag{3}$$

Equation (3) contains all diffracted orders, including the transmitted beams. In thin-film (Raman–Nath) diffraction, the first diffraction order occurs for $m = 1$, and the diffracted field amplitude is

$$E_d(\omega) = E_{\text{in}}(\omega)\exp(i\tilde{n}kL) iJ_1(\Delta\tilde{n}kL)\exp(iKx + \phi), \tag{4}$$

which for small grating amplitudes be written as

$$\begin{aligned} E_d(\omega) &= {}^1/_2 E_{\text{in}}(\omega)\exp(i\tilde{n}kL)(\Delta\tilde{n}kL) \\ &= {}^1/_2 E_{\text{in}}(\omega)\exp(i\tilde{n}kL)\left(\Delta nkL + i\frac{\Delta\alpha L}{2}\right), \end{aligned} \tag{5}$$

where we have used the approximation $J_m(z) \cong (z/2)^2/m!$ for small z. Note that the diffracted pulse acquires a spectrally dependent phase (the excitonic spectral phase) $\theta(\omega)$, defined as

$$\tan\theta(\omega) = \frac{\Delta\alpha(\omega)}{2k\Delta n(\omega)}. \tag{6}$$

The diffracted intensity is proportional to

$$\begin{aligned} |E_d(\omega)|^2 = \frac{1}{4}|E_{\text{in}}(\omega)|^2 \exp(-\alpha L) \\ \times \left\{[\Delta n(\omega)]^2 + \left[\frac{\Delta\alpha(\omega)}{2k}\right]^2\right\}(kL)^2. \end{aligned} \tag{7}$$

Two quantities can be defined to characterize the diffraction efficiency of the device. The ratio $\eta_{\text{in}} = |E_d(\omega)|^2/|E_{\text{in}}(\omega)|^2$ between the diffracted and the incident beam intensities is the input diffraction efficiency. Output diffraction efficiency η_{out} is defined as the ratio of the diffracted and the transmitted beams on the device and depends only on the electrorefraction and electroabsorption spectra:

$$\begin{aligned} \eta_{\text{out}}(\omega) &= {}^1/_4|kL\Delta\tilde{n}(\omega)|^2 \\ &= {}^1/_4\{[\Delta n(\omega)kL]^2 + [\Delta\alpha(\omega)L/2]^2\}. \end{aligned} \tag{8}$$

In a typical PRQW,[20] the diffraction is limited to a 3–4 nm range about the heavy-hole exciton transition. To achieve diffraction of pulses with durations of 100 fs or shorter without considerable bandwidth narrowing requires broadening of the spectral distribution of the complex electrorefraction, $\Delta\tilde{n}(\omega)$. This amounts to specifically designing the spectral distribution of the excitonic oscillator strength.

There are two possible approaches to the problem of engineering the density of states in quantum wells. In the first approach, when there is coupling between the wells,

the superlattice exhibits a dense spectrum of critical points, which has associated with it a dense distribution of excitonic transition energies. One implementation of this idea is quasi-periodic (Fibonacci) superlattices, in which spatial quasi-periodicity leads to a dense and fractal set of excitonic transitions.[21] However, the usefulness of such structures as broadband devices is limited by the concentration of oscillator strength to the low-energy edge of the miniband,[22,23] which results in bandwidths comparable with those of standard quantum wells.

Here we take an approach to designing a broad spectrum of excitonic transitions that relies on the grading of the quantum confinement of the carriers in isolated quantum wells along the growth direction of the device. This simple process constitutes a controlled inhomogeneous broadening of the excitonic transition. Its implementation is however not trivial because of the dependence of the electro-optic response on a number of factors, such as exciton oscillator strength and exciton sensitivity to the applied electric field, which in turn depend on the exciton linewidth and the exciton binding energy. A realistic device design has to take into account the variation of these parameters with carrier confinement, or well width.

We can achieve the grading of carrier quantum confinement most easily by modulating either the confining potential (barrier heights) or the well widths. In this case the electro-optic response of the quantum-well device is a convolution over the individual quantum wells or, equivalently, along the direction normal to the wells (growth direction), y:

$$\Delta\tilde{n}_{\mathrm{TOT}}(\omega) = \int \Delta\tilde{n}(\omega, y) g(y)\mathrm{d}y, \tag{9}$$

where the distribution function of quantum-well types $g(y)$ is normalized: $\int g(y)\mathrm{d}y = 1$. This equation is subject to physical conditions. An important physical constraint is the concentration of oscillator strength in excitonic transitions to the low-energy side of the their spectrum whenever there is Coulomb interaction between carriers in extended states, as in the case of superlattices.[22] This effect precludes simple designs, such as that of a graded gap epilayer. Also, a distribution of quantum wells with linearly varying transition energy could not yield large bandwidths because the exciton oscillator strength is conserved on broadening, and Eq. (9) integrates to zero through the center of the distribution.

If the distribution of change in index $\Delta\tilde{n}(\omega, y)$ is known as a function of well widths or barrier heights, integral equation (9) is an inverse problem for the function $g(y)$, with the constraint that $g > 0$. Because of this, the inversion of Eq. (9) is not a simple problem, and in practice one must use other methods, such as iterative procedures, to arrive at a distribution function close to the solution. Once the amplitude of the desired diffraction efficiency $|\Delta\tilde{n}(\omega)|$ is known, the real and imaginary parts of the electrorefraction are fixed by the Kramers–Kronig relations and can be determined from the excitonic spectral phase, given by[24]

$$\theta(\omega) = -\frac{2\omega}{\pi}\mathcal{P}\int_0^{+\infty} \frac{\ln|\Delta\tilde{n}(\omega')|}{\omega'^2 - \omega^2}\mathrm{d}\omega', \tag{10}$$

where $\mathcal{P}$ signifies the principal value of the integral. Therefore a desired diffraction spectrum uniquely determines a spectral distribution of electrorefraction, which in turn can be inverted by use of Eq. (9) to yield a specific device design. This signifies that arbitrary bandwidth can be designed with quantum-well devices, a condition that can be useful in pulse-shaping applications.

In the structure shown in cross section in Fig. 1, the well widths have been adjusted in four discrete monolayer steps to modulate the heavy-hole exciton transition wavelength over a 4.5-nm range. The device consists of four multiwell segments of GaAs/$Al_{0.3}Ga_{0.7}As$ quantum wells. The well widths were 76.4, 73.6, 70.8, and 67.9 Å (1 Å = 0.1 nm), corresponding to 25, 26, 27, and 24 monolayers, and with repetitions, respectively, of 6, 12, 18, and 16 periods. The barriers were uniformly 100 Å wide. The $Al_{0.5}Ga_{0.5}As$ and AlAs layers serve as stop-etch layers used in the chemical etching of the opaque GaAs substrate.[20] For this device, the distribution function $g(y)$ is simply a sum of four step (Heaviside) functions with variable step size. The device operates in transmission, under an applied electric field parallel to the quantum wells. The well widths were chosen to be integral multiples of GaAs atomic monolayers. Therefore the device was not optimized for a spectrally flat diffraction efficiency, which would require a continuous distribution of (fractional monolayer) well widths.

The absorption and differential transmission spectra of the broadband device are shown in Fig. 2 along with the corresponding curves for a standard MQW device. The absorption and differential transmission measurements were performed with a tungsten lamp as the incoherent-light source and with a double-pass monochromator and lock-in detection. The heavy-hole transition wavelengths for the individual four layers of the broadband device are indicated in the figure. The spectral features that are due to the various discrete excitonic levels cannot be distinguished in the absorption and differential transmission spectra shown in Fig. 2; apart from their having a wider spectral extension, these spectra are similar to the corresponding spectra of the standard narrow-band quantum-well device. The electroabsorption and elec-

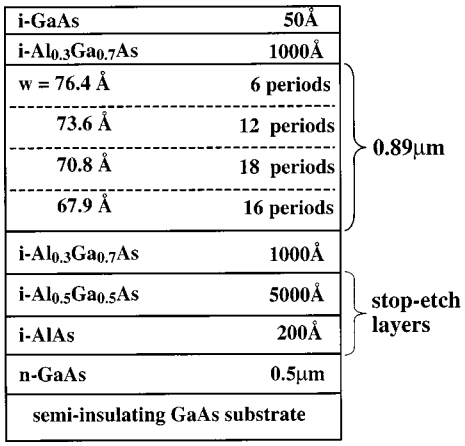

Fig. 1. Cross section of the four-layer MQW device, with the widths of the quantum wells explicitly indicated. The GaAs well widths range from 24 to 27 monolayers. All barriers were 100-Å $Al_{0.3}Ga_{0.7}As$.

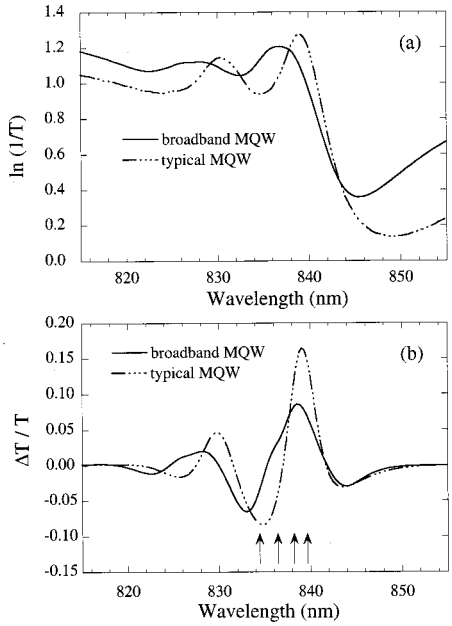

Fig. 2. (a) Absorption coefficient for the broadband device and for a standard MQW device (60 periods of 75-Å GaAs/100Å $Al_{0.3}Ga_{0.7}As$ quantum wells). (b) Differential transmission for the broadband MQW (under an applied field of 10 kV/cm) and for the standard MQW (under 8 kV/cm) in the transverse Franz–Keldysh geometry.

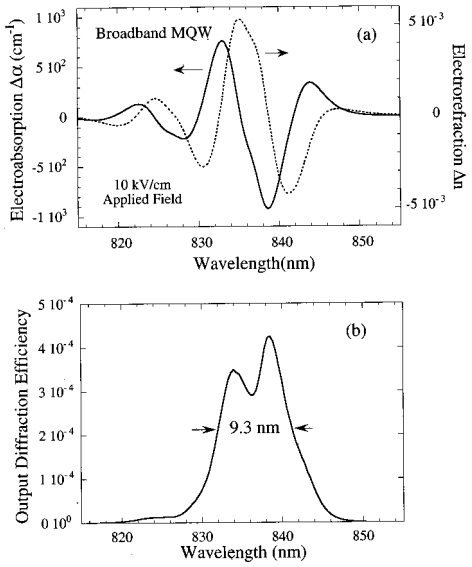

Fig. 3. (a) Change in absorption coefficient and in index of refraction of the broadband device for an applied electric field of 10 kV/cm. (b) Calculated output diffraction efficiency for the same applied field.

trorefraction of the broadband structure that are due to an applied field of 10 kV/cm are presented in Fig. 3(a). The strong variations and oscillations of the electroabsorption would in general be expected to distort and chirp the diffracted pulse, as we discuss in Section 4 below. Figure 3(b) shows the predicted output diffraction efficiency, calculated from the electroabsorption data by use of Eq. (8). The device was designed for a diffraction efficiency bandwidth comparable with the bandwidth of the ultrashort pulses used in our experiments but was not optimized for a flat spectral dependence of the diffraction efficiency: The double peak at the maximum of the diffraction efficiency spectrum is due to the monolayer discreteness of the distribution function $g(y)$ chosen in our design.

3. FOUR-WAVE MIXING CHARACTERIZATION

To characterize femtosecond pulse diffraction from the broadband structure, we performed degenerate four-wave mixing measurements,[4] using ultrashort pulses generated by a mode-locked Ti:sapphire laser with nominal pulse durations of 100 fs. The approximately Gaussian incident pulses have a bandwidth of 8.8 nm and a duration of ≈110 fs. These values correspond to a time–bandwidth product of 0.414, which is indicative of nearly transform-limited pulses.

In the four-wave mixing experiments the grating fringe spacing was fixed at 20.6 μm and the total incident intensity was 5 mW/cm^2, with a beam ratio close to unity. The applied electric field was 10 kV/cm. The diffraction spectra for two different input central wavelengths are λ_c = 834.5 nm [Fig. 4(a)] and 840.0 nm [Fig. 4(b)]. The bandwidth and the spectral shape of the diffracted beam can be adjusted by tuning of the central wavelength of the incident pulses. The diffracted bandwidth of 8.3 nm in Fig. 4(a) is close to the bandwidth of the incident pulse; however, we do not expect the diffracted pulse to be transform limited, because the input diffraction efficiency was not flat across the input pulse spectrum.

To characterize the time dependence of the diffracted and transmitted pulses we used electric-field cross correlation between the signal pulse and a known (transform-limited) reference pulse. Electric-field cross correlation has the advantage that it can be used to characterize the low diffracted pulse powers available in our experiments.

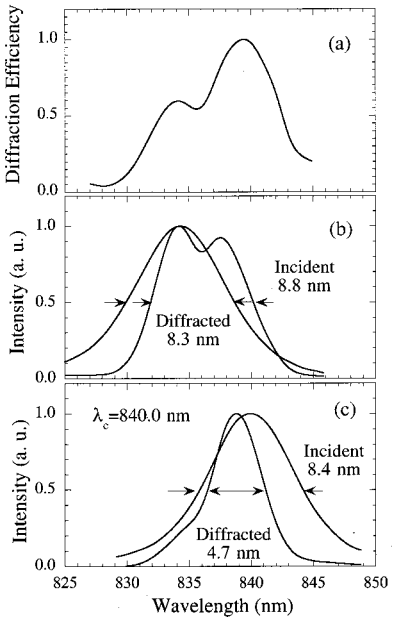

Fig. 4. (a) Measured input diffraction efficiency in degenerate four-wave mixing. (b), (c) Spectra of the incident and diffracted pulses for incident pulses centered about 834.5 and 840.0 nm.

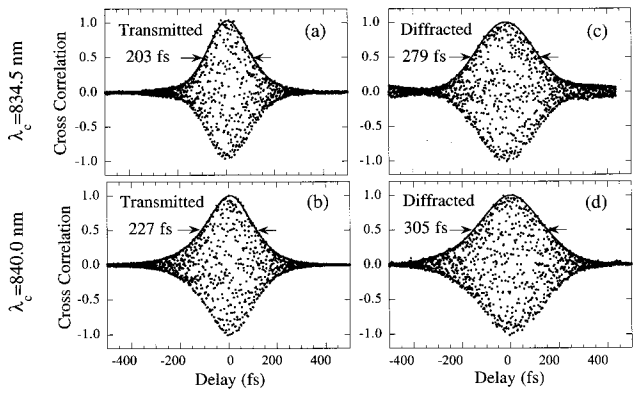

Fig. 5. (a), (b) Electric-field cross correlations of the transmitted pulse against the reference pulse for two central wavelengths of the incident pulse and (c), (d) the electric-field cross correlation of the diffracted pulses with the reference pulse for the corresponding value of λ_c.

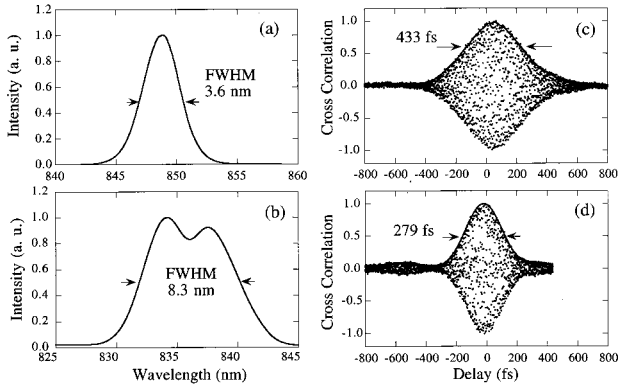

Fig. 6. Diffracted spectra of (a) a single-layer MQW device (from Ref. 4) and (b) the four-layer broadband device. The corresponding electric-field cross-correlation traces for (c) the single MQW and (d) the broadband structure are also shown.

In electric-field correlation, a signal pulse interferes with a reference pulse delayed by a (variable) time τ, and the average measured intensity is

$$I_{x\mathrm{corr}}(\tau) = 1_{\mathrm{sig}} + I_{\mathrm{ref}} + 2\sqrt{I_{\mathrm{sig}} I_{\mathrm{ref}}}\,\mathrm{Re} \times \left[\exp(-i\omega_c\tau)\int e_{\mathrm{sig}}(t)e_{\mathrm{ref}}{}^*(t-\tau)\mathrm{d}t\right], \quad (11)$$

where the correlation function $\gamma_{s,r}(\tau) = \int e_{\mathrm{sig}}(t)e_{\mathrm{ref}}{}^*(t-\tau)\mathrm{d}t$ contains information about the time dependence of the signal pulse. The FWHM of the correlation $\tau_{s,r} = [2(\tau_{\mathrm{sig}}{}^2 + \tau_{\mathrm{ref}}{}^2)]^{1/2}$ can be used to extract the signal pulse duration when both pulses are transform limited.

The electric-field cross correlations of the transmitted and diffracted pulses for the two central wavelengths are shown in Fig. 5. We achieved the time delay between the diffracted (transmitted) and the reference pulses by using a motorized translation stage with a resolution of 0.1 μm. The width of the electric-field cross-correlation trace for the diffracted pulse centered about 840.0 nm is consistent with a pulse duration of 185 fs, corresponding to broadening by a factor of 1.7, whereas the cross-correlation width for diffracted pulses centered about 834.5 nm is consistent with a pulse duration of 164 fs, which represents a broadening of the incident pulses by a factor of approximately 1.5.

To compare the diffractive performance of the broadband four-layer device with that of a standard MQW device with one type of quantum well, we show in Fig. 6 the diffraction spectra and electric-field cross correlation for the four-layer device and for a GaAs/GaAs/$Al_{0.1}Ga_{0.9}As$ MQW device from Ref. 4. The bandwidth of the broadband structure is 2.3 times larger, and the duration of the pulse, extracted from the cross-correlation width, is 1.8 times shorter than for the standard structure. The pulses diffracted from the standard MQW device were shown[4] to be nearly transform limited, with a flat spectral phase. This property is desirable from the point of view of using MQW photorefractive devices in femtosecond applications, and in Section 4 we explain why we expect the spectral phase of the diffracted pulse to be nearly linear for any MQW device.

4. SPECTRAL INTERFEROMETRY AND EXCITONIC SPECTRAL PHASE

The spectral phase of the diffracted pulses can be measured by spectral interferometry. Spectral interferometry is the analog in the frequency domain of electric-field cross correlation, and in practice the spectral resolution is sufficient to ensure signal pulse retrieval. For a fixed delay τ between the signal and the reference pulses, the oscillatory part of the spectrogram obtained by interfering the signal and reference pulses is

$$S(\omega,\tau) = I_{\mathrm{TOT}}(\omega,\tau) - I_{\mathrm{sig}}(\omega) - I_{\mathrm{ref}}(\omega) \equiv 2\,\mathrm{Re}[e_{\mathrm{sig}}(\omega)e_{\mathrm{ref}}{}^*(\omega)\exp(-i\omega\tau)], \quad (12)$$

where $e_{\mathrm{sig}}(\omega)$ stands for the Fourier transform of $e_{\mathrm{sig}}(t)$. If the spectral phase of the reference pulse is known, the positions of the peaks in the interferogram [Eq. (12)] contain information about the phase of the signal pulse, and therefore both the spectral amplitude and phase of the signal pulse can be extracted.

The spectral interferograms for the transmitted and diffracted pulses are shown in Fig. 7, together with the extracted phases. The linear spectral dependence of the phase, which leads only to a delay in time and does not

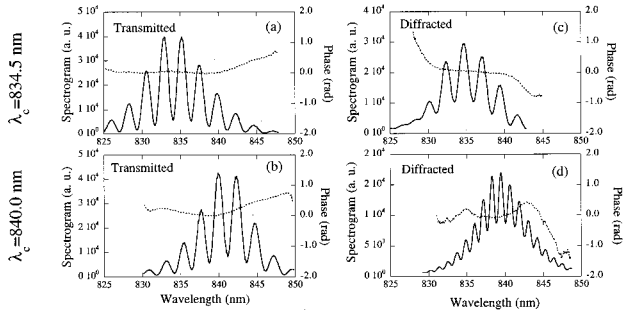

Fig. 7. (a), (b) Spectral interoferograms and extracted phases of the transmitted spectra with the reference pulse spectrum for two central wavelengths of the incident pulse and (c), (d) the curves for the corresponding values of λ_c. The delay between the measured and the reference pulses was 1.0 ps for all interferograms except for (d), for which it was 2.0 ps.

distort the pulses, has been subtracted out. The spectral phases of both transmitted pulses are nearly independent of wavelength near the excitonic transition, with small (< 0.2-rad) phase variation across the center of the transmitted spectrum, consistent with the fact that the transmitted pulses experience little broadening. The spectral phase of the diffracted pulses shows stronger variation with wavelength, mainly in the wings of the diffracted spectra, but still smaller than 0.5 rad across the center of the spectrum. For the incident pulse centered about 834.5 nm, the quadratic (5.4×10^{-3}-rad/nm^2) and the larger cubic (1.9×10^{-3}-rad/nm^3) terms in the spectral phase of the diffracted pulses lead to relatively small phase distortions.

The spectral phase of the diffracted pulse, defined in Eq. (6), varies by $\sim 5.5\pi$ across the heavy- and light-hole transitions. However, this variation is mostly linear in wavelength (as shown in Fig. 8) and thus leads to a time delay with little distortion for diffracted femtosecond pulses. Because a diffracted phase with large nonlinear terms (quadratic or higher order) leads to chirped pulses, it is important to know whether the small contribution of higher-order phase terms in the diffracted pulses in our experiments is a coincidence or a general property of quantum-well devices.

The wavelength dependence of the excitonic spectral phase is determined by the Kramers–Kronig relations and causality,[24] which connects the real and the imaginary parts of the complex electrorefraction $\Delta\tilde{n}(\omega)$. To estimate the degree to which the excitonic spectral phase is linear in wavelength, we can write the imaginary part of the electrorefraction as a sinusoidal function in frequency with a slowly varying amplitude $A(\omega)$ and a slowly varying phase factor $\varphi(\omega)$:

$$\mathrm{Im}(\Delta\tilde{n}) = A(\omega)\cos[\omega\kappa + \varphi(\omega)], \tag{13}$$

with κ a constant. Because of the oscillatory nature of the electroabsorption as a function of wavelength, this is a good approximation, as shown by the dotted curve in Fig. 8. The electrorefraction can be written as a Hilbert transform:

$$\mathrm{Re}[\Delta\tilde{n}(\omega)] = \frac{1}{\pi}\mathcal{P}\int_{-\infty}^{+\infty}\frac{\mathrm{Im}[\Delta\tilde{n}(\omega')]}{\omega' - \omega}\,\mathrm{d}\omega'. \tag{14}$$

The derivative of Eq. (14) with respect to frequency is

$$\frac{\partial}{\partial\omega}\mathrm{Re}[\Delta\tilde{n}(\omega)] = \frac{1}{\pi}\mathcal{P}\int_{-\infty}^{+\infty}\frac{\mathrm{Im}[\Delta\tilde{n}(\omega')]}{(\omega' - \omega)^2}\,\mathrm{d}\omega' \propto \mathrm{Im}[\Delta\tilde{n}(\omega)], \tag{15}$$

because the denominator is a sharply peaked function about ω and can be approximated by a Dirac δ function.[25] A similar relationship holds for the derivative of the imaginary part of the index. Therefore the real part of the electrorefraction is approximately proportional to the derivative of the imaginary part and vice versa, as can be seen from Fig. 8. In consequence, the excitonic spectral phase from Eq. (6) can be written as

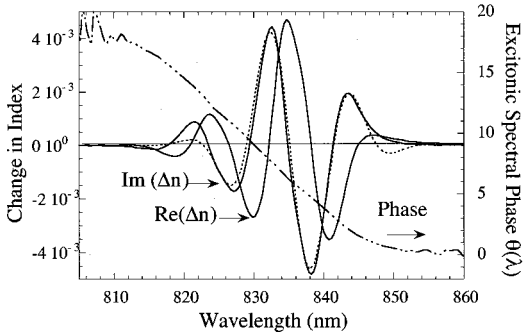

Fig. 8. Changes in the real and the imaginary parts of the refractive index under an applied electric field [under the same conditions as for Fig. 3(a)] plotted together with the excitonic spectral phase $\theta(\omega)$. The imaginary part of $\Delta\tilde{n}$ is derived from electroabsorption data; the real part is calculated through a Kramers–Kronig transform. The excitonic spectral phase is mostly linear in wavelength, although it varies by 5.5π rad across the heavy- and light-hole transitions. The slowly varying amplitude and phase approximation for the electroabsorption [Eq. (14)] is shown by the dotted curve.

$$\tan[\theta(\omega) + \pi/2] \cong \tan[\omega\kappa + \varphi(\omega)]\left(1 + \frac{1}{\kappa}\frac{\partial\varphi}{\partial\omega}\right) - \frac{1}{\kappa A}\frac{\partial A}{\partial\omega}. \tag{16}$$

The deviations from linearity of the spectral phase are determined by the terms $(1/\kappa)$ $(\partial\varphi/\partial\omega)$ and $(1/\kappa\mathrm{A})$ $(\partial\mathrm{A}/\partial\omega)$ in relation (16). In typical MQW devices the energy difference between the heavy- and light-hole transitions and the exciton linewidth are such that Eq. (13) is a good approximation and these terms are small (in our case, both are everywhere smaller than 0.125); therefore the spectral phase is linear to a high degree. The capability to design broadband photorefractive MQW devices is therefore limited neither by the bandwidth of the diffraction spectrum, which can in principle be designed to have arbitrary bandwidths and line shapes, nor by the requirement that the diffracted pulses be transform limited.

5. CONCLUSIONS

We have demonstrated broadband, low-dispersion diffraction from suitably designed photorefractive multiple-quantum-well devices. The low quadratic dispersion of the diffracted pulses is due to the fact that the real and the imaginary parts of the electro-optic response of the photorefractive quantum wells form an approximate sinusoidal Hilbert-transform pair. Dispersion-free diffraction is a general property of multiple-quantum-well devices and opens the possibility of engineering arbitrary diffraction spectra. The wide range of operating wavelengths, diffraction bandwidths, and diffraction line shapes attainable through bandgap engineering, together with the linearity of the diffracted spectral phase, makes photorefractive quantum wells candidates for broadband dynamic holographic materials with potential use in pulse-shaping and spectral holography applications.

ACKNOWLEDGMENT

The authors gratefully acknowledge support by National Science Foundation grant ECS-9708230.

REFERENCES

1. D. D. Nolte and M. R. Melloch, "Photorefractive quantum wells and thin films," in *Photorefractive Effects and Materials*, D. D. Nolte, ed. (Kluwer Academic, Dordrecht, The Netherlands, 1995).
2. A. M. Weiner, J. P. Heritage, and E. M. Kirschner, "High-resolution femtosecond pulse shaping," J. Opt. Soc. Am. B **5**, 1563–1572 (1988).
3. A. M. Weiner, D. E. Leaird, D. H. Reitze, and E. G. Paek, "Femtosecond spectral holography," IEEE J. Quantum Electron. **28**, 2251–2261 (1992).
4. R. M. Brubaker, Y. Ding, D. D. Nolte, M. R. Melloch, and A. M. Weiner, "Bandwidth-limited diffraction of femtosecond pulses from photorefractive quantum wells," IEEE J. Quantum Electron. **33**, 2150–2158 (1997).
5. Y. Ding, R. M. Brubaker, D. D. Nolte, M. R. Melloch, and A. M. Weiner, "Femtosecond pulse shaping by dynamic holograms in photorefractive quantum wells," Opt. Lett. **22**, 718–720 (1997).
6. Y. Ding, D. D. Nolte, M. R. Melloch, and A. M. Weiner, "Real-time edge enhancement of femtosecond time-domain images by use of photorefractive quantum wells," Opt. Lett. **22**, 1101–1103 (1997).
7. Y. Ding, D. D. Nolte, and A. M. Weiner, "Adaptive all-order dispersion compensation of ultrafast laser pulses using dynamic spectral holography," Appl. Phys. Lett. **75**, 3255–3257 (1999).
8. R. Jones, M. Tziraki, P. M. W. French, K. M. Kwolek, D. D. Nolte, and M. R. Meloch, "Direct-to-video holographic 3-D imaging using photorefractive multiple quantum well devices," Opt. Express **2**, 439–448 (1998); http://epubs.osa.org/optics express.
9. R. Jones, N. P. Barry, S. C. W. Hyde, M. Tziraki, J. C. Dainty, P. M. W. French, D. D. Nolte, K. M. Kwolek, and M. R. Melloch, "Real-time 3-D holographic imaging using photorefractive media including multiple-quantum-well devices," IEEE J. Sel. Top. Quantum Electron. **4**, 360 (1998).
10. W. S. Rabinovich, M. Bashkansky, S. R. Bowman, R. Mahon, and P. R. Battle, "Speckle photography using optically addressed multiple quantum well spatial light modulators," Opt. Express **2**, 449–453 (1998): http://epubs.osa.org/opticsexpress.
11. I. Lahiri, L. J. Pyrak-Nolte, and D. D. Nolte, "Laser-based ultrasound detection using photorefractive quantum wells," Appl. Phys. Lett. **73**, 1041–1043 (1998).
12. Y. Ding, D. D. Nolte, M. R. Melloch, and A. M. Weiner, "Time-domain image processing using dynamic holography," IEEE J. Sel. Top. Quantum Electron. **4**, 332–341 (1998).
13. J. Glesk, K. I. Kang, and P. R. Prucnal, "Ultrafast photonic packet switching with optical control," Opt. Express **1**, 1997.
14. W. S. Warren, H. Rabitz, and M. Dahleh, "Coherent control of quantum dynamics: the dream is alive," Science **259**, 1581–1589 (1991).
15. M. R. Fetterman, D. Goswami, D. Keusters, W. Yang, J.-K. Rhee, and S. Warren, "Ultrafast pulse shaping: amplification and characterization," Opt. Express **3**, 366–375 (1998); http://epubs.osa.org/opticsexpress.
16. E. S. Maniloff, D. Vacar, D. W. McBranch, H.-L. Wang, B. R. Mattes, J. Gao, and A. J. Heeger, "Ultrafast holography using charge-transfer polymers," Opt. Commun. **141**, 243–246 (1997).
17. J. S. Aitchinson, A. H. Kean, C. N. Ironside, A. Villeneuve, and G. I. Stegeman, "Ultrafast all-optical switching in $Al_{0.18}Ga_{0.82}As$ directional coupler in the 1.55 μm spectral region," Electron. Lett. **27**, 1709–1710 (1991).
18. G. R. Jacobovitz-Veselka, U. Keller, and M. T. Asom, "Broadband fast semiconductor saturable absorber," Opt. Lett. **17**, 1791–1793 (1992).
19. L. R. Brovelli, U. Keller, and T. H. Chiu, "Design and operation of antiresonant Fabry–Perot saturable semiconductor absorbers for mode-locked solid-state lasers," J. Opt. Soc. Am. B **12**, 311–313 (1995).
20. Q. Wang, R. M. Brubaker, D. D. Nolte, and M. R. Melloch, "Photorefractive quantum wells: transverse Franz–Keldysh geometry," J. Opt. Soc. Am. B **9**, 1626–1641 (1992).
21. M. Dinu, M. Melloch, and D. D. Nolte, "Electro-optic and photorefractive properties of long-period Fibonacci superlattices," J. Appl. Phys. **79**, 3787–3789 (1996).
22. H. Chu and Y.-C. Chang, "Saddle-point excitons in solids and superlattices," Phys. Rev. B **36**, 2946–2949 (1987).
23. M. Dinu, D. D. Nolte, and M. R. Melloch, "Electroabsorption spectroscopy of effective-mass $Al_xGa_{1-x}As$/GaAs Fibonacci superlattices," Phys. Rev. B **56**, 1987–1995 (1997).
24. P. Y. Yu and M. Cardona, *Fundamentals of Semiconductors* (Springer-Verlag, Berlin, 1996).
25. J. D. Jackson, *Classical Electrodynamics* (Wiley, New York, 1975).